water

MDPI

Article

Numerical and Physical Modeling to Improve Discharge Rates in Open Channel Infrastructures

Rick Jaeger [1,*], Katharina Tondera [2], Carolyn Jacobs [1], Mark Porter [1] and Neil Tindale [1]

1 School of Science and Engineering, University of the Sunshine Coast, Sippy Downs, QLD 4556, Australia
2 IMT Atlantique Bretagne—Pays de Loire, Department of Energy Systems and Environment, 44307 Nantes, France
* Correspondence: rjaeger@usc.edu.au

Received: 6 June 2019; Accepted: 8 July 2019; Published: 10 July 2019

Abstract: This paper presents the findings of a study into how different inlet designs for stormwater culverts increase the discharge rate. The objective of the study was to develop improved inlet designs that could be retro-fitted to existing stormwater culvert structures in order to increase discharge capacity and allow for changing rainfall patterns and severe weather events that are expected as a consequence of climate change. Three different chamfer angles and a rounded corner were simulated with the software ANSYS Fluent, each of the shapes tested in five different sizes. Rounded and 45° chamfers at the inlet edge performed best, significantly increasing the flow rate, though the size of the configurations was a critical factor. Inlet angles of 30° and 60° caused greater turbulence in the simulations than did 45° and the rounded corner. The best performing shape of the inlet, the rounded corner, was tested in an experimental flume. The flume flow experiment showed that the optimal inlet configuration, a rounded inlet (radius = 1/5 culvert width) improved the flow rate by up to 20% under submerged inlet control conditions.

Keywords: culvert; culvert design; culvert hydraulics; culvert retrofitting; discharge capacity; inlet optimization; ANSYS Fluent

1. Introduction

Culverts have a key function in our transport infrastructure, as their simple design allows for safe crossings of waterways. The size and designs of culverts are calculated using discharge estimates based on historical rainfall data and hydraulic equations that determine headwater levels. Modern design guidelines of stormwater culverts are based on research from the 1950s and 1960s conducted in the U.S. by French [1–6] and others [7,8]. These studies tested a variety of culvert configurations in laboratory models, and other research investigated loss coefficients, aquatic organism passage and culvert blockages [9–12] and informed the design guidelines used today (e.g., [13–15]). Several factors influence the discharge capacity of a culvert, but the cross-sectional area and the inlet configuration are the two that can be controlled the easiest with the biggest impact on water flow. The importance and benefits of well-designed inlets were recognized in early research [16], yet modern design guidelines have failed to adopt these benefits [17–21]. A review of the geometric influence on hydraulic performances in rectangular culverts was completed in 2004 by Jones et al. [19]; but only a few sizes of the inlet design were investigated, and most subsequent alterations were limited to the top bevel and/or wingwall setups rather than to the shape of the complete opening. Since then, few publications have discussed culvert inlets [20–24], and none have focused on discharge improvements.

Minimum energy loss (MEL) culverts [9,25] have a streamlined design and maintain flow in subcritical conditions. This is a more complex geometry than the one used in a normal culvert and the unique design of every structure does not allow its transfer to already existing culverts. However, the principle of minimizing energy losses caused by the structure itself can be transferred and could help to deal with new challenges that the stormwater infrastructure is facing. Changes in rainfall patterns due to global warming pose a great threat to culverts that, once installed, are expected to function for many years [26–30]. More intense rainfall events in the future pose a threat to smaller stream crossings where culverts are the preferred solution rather than bridges [19,31–34]. Overflows, as a result of higher discharge rates than can be accommodated by culverts, can damage the structure, as well as areas upstream of the culvert and reduce the overall reliability of the road and stream crossing. To mitigate these risks, the capacity of many culverts needs to be increased, particularly under high flow conditions. Performance improvements, such as retrofitting of sharp corners at the inlet, would represent a more economical solution than completely replacing existing culverts with larger pipes.

Instead of testing new ideas/modifications empirically, hydraulic simulations with numeric computation have become a popular alternative with the advent of greater computer speeds and storage. Computational fluid dynamics (CFD) has been used previously to solve a variety of culvert-related research questions [11,12], but not those associated with hydraulic optimization of the inlet.

2. Methods

This study investigated four different inlet improvements for culverts to increase their performance. Twenty-one different setups were modelled with ANSYS Fluent software [35], and the most promising configuration was tested in an experimental flume.

2.1. Simulation Setup

Stormwater culverts were represented in two-dimensions (Figure 1), with a large rectangle (representing the upstream water body) connected directly to the culvert. All simulations used the same dimensions, and only the inlet corners of the culvert were changed. The flow medium was chosen from the Fluent database as liquid water at 20 °C. As the impact of inlet geometries was the focus of this investigation, a material with low friction (aluminium) was chosen as the wall material. Rectangular corners at the inlet (inlet type: square) were used as a standard configuration and compared against chamfered and rounded inlet improvements (Table 1). Chamfered improvements were separated into three different angles, each with five different lengths, measured at the side that connects to the culvert. Rounded improvements were tested using five different sizes of quadrants connected tangentially to the inlet.

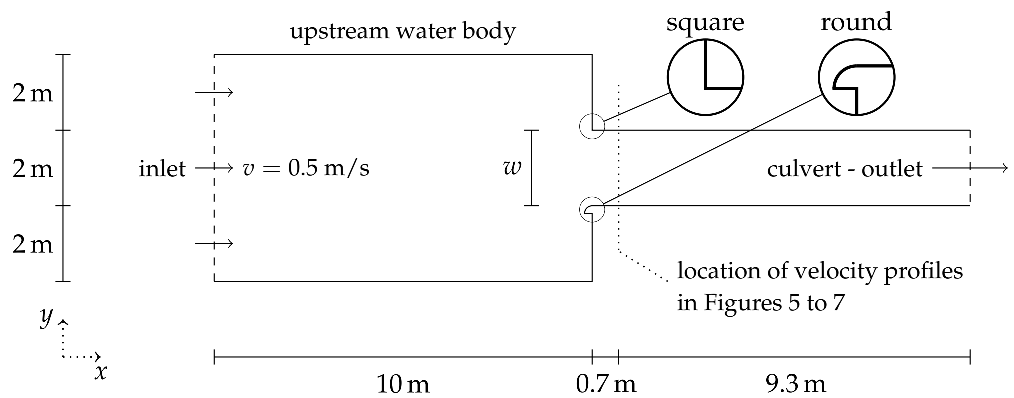

Figure 1. Overview of the 2D simulation model; v = velocity, w = width of the culvert; the square and round corner are examples of the applied modifications.

Table 1. Geometry and nomenclature declaration for CFD analysis; α: angle, l: length, r: radius, w: width of the culvert.

Inlet Type	Configurations	Abbreviation
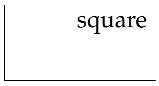 square	none	*square*
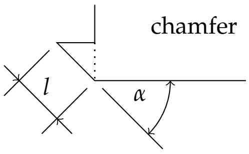 chamfer	$\alpha = \{30°, 45°, 60°\}$ $length = 0.05\,w,\ 0.10\,w, \ldots, 0.25\,w$	$\alpha\ (length)$
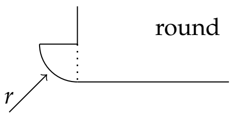 round	$radius = 0.05\,w,\ 0.10\,w, \ldots, 0.25\,w$	$R\ (radius)$

The entire model surface was defined as a fluid body with an inflow velocity of $0.5\,\mathrm{m\,s^{-1}}$ and atmospheric conditions of zero pressure at the outlet. The meshing configurations are summarized in Appendix A, Table A1. Unless indicated otherwise in Table A1, standard parameters were chosen. The generated mesh was further refined and repaired with the help of ANSYS Fluent until an orthogonal quality above 0.9 and a mesh skewness below 0.1 were achieved. All simulations were solved as steady-state scenarios until convergence.

The $k-\epsilon$ model was used in all scenarios to account for turbulence. It used the Reynolds averaged Navier–Stokes (RANS) equation, where the turbulence is modelled with mean and fluctuating components, resulting in an equation that consists of the Navier–Stokes equation with additional (time-averaged) Reynolds stresses: $\rho\overline{u_i'u_j'}$. Velocities and scalar quantities were decomposed into a time averaged component ($\overline{u}_i$) and a fluctuating component (u_i'). To calculate the Reynolds stresses, Boussinesq [36] introduced the concept of eddy viscosity, where turbulence stresses are related to the mean flow. In the $k-\epsilon$ model, the turbulent kinetic energy k and the isotrope dissipation rate ϵ [37] are used to calculate the introduced eddy viscosity with two partial differential equations.

The $k-\epsilon$ model is widely used in CFD simulations, but it oversimplifies any stress as isotropic, which is not the case in areas close to walls. These limitations result in an inability to calculate near-wall effects correctly, such as highly-swirling or stress-driven secondary flows [38]. As the macro-geometry effects, rather than the low-Reynolds-number effects from the viscous sublayer and the blending region were the focus of these simulations, the $k-\epsilon$ model was deemed to be most appropriate. To further mitigate the effects of these limitations, several countermeasures were adopted. Firstly, so-called standard wall functions were used to describe fluid behaviour close to walls. Launder and Spalding proposed this concept with multiple constants to expand the usability of the $k-\epsilon$ model [39]. Secondly, a low friction material and a refined grid along the points of interest were used to minimize expected inaccuracies.

Once the simulations were completed, the streamlines, velocity fields and areas of turbulence from each simulation were compared in order to rate the influence of each inlet configuration. A small vena contracta is preferable: few areas with very high or very low velocities and little turbulence. After a visual result comparison, absolute flow values were compared. The cross-sectional area where the greatest constriction occurred was chosen as a point of interest. After identifying the distance from the inlet to the greatest constriction in every setup, the arithmetic mean was calculated from the collected lengths ($\bar{d} = 0.74\,\mathrm{m}$) to define the sampling point. At 0.7 m after the headwall, a flow profile was taken from every setup to compare explicit velocity values directly.

2.2. Experimental Setup

An experimental flume was used to test the flow improvements from the simulations. A Perspex culvert model was placed in the centre of a 5 m-long by 0.6 m-wide channel, with the opening 20 mm above ground. The circular culvert model (pipe length: 100 mm, inner diameter: 105 mm) was integrated into a sheet of Perspex, resulting in a flush, rectangular inlet corner. Two different inlet shapes were tested: a square edge with a headwall and a rounded inlet (Table 1, inlet type square and round). A 3D printer with a fused filament fabrication process [40] was used to create the rounded inlet modification. The 20 mm radius was approximately 20 % of the culvert size and surrounded the slightly elevated inlet of the culvert. The depth of the flume allowed headwater heights up to 0.6 m with little turbulence, as the water entered through a submerged overflow inlet (Figure A1). The flow rate was controlled by a variable-speed drive and measured with a magnetic flowmeter (WaterMaster FEX100, ABB Australia) before it entered the flume. The maximum error for this flowmeter, as determined by the manufacturer, was <1 % for flow rates from 1 L s^{-1} to 20 L s^{-1}. Headwater depth measurements were taken with a ruler (accuracy 1 mm) five minutes after each flow rate change to ensure enough time for the headwater levels to stabilize.

3. Results

3.1. Numerical Simulation Results

Streamlines visualize flow paths in fluids. They are tangential to the velocity vectors and depict the vector length using various colours. Streamlines (Figure A2) were calculated from the inlet and highlighted the constriction at the inlet caused by the vena contracta, where the cross-sectional area of flow was at its minimum. The greater the flow constriction (vena contracta), the poorer the performance. This is presented in Table 2 as a measure of the remaining cross-sectional area in the culvert: the bigger the remaining flow area, the better the flow through the culvert.

Table 2. Remaining flow areas from the streamline visualization.

	Size					
	-	**0.05 w**	**0.10 w**	**0.15 w**	**0.20 w**	**0.25 w**
square	0.64	-	-	-	-	-
30°	-	0.64	0.70	0.76	0.84	0.87
45°	-	0.65	0.70	0.84	0.87	0.88
60°	-	0.67	0.81	0.82	0.82	0.84
round	-	0.68	0.81	0.89	0.91	0.92

This shows that the performance of very small inlet configurations changes (0.05 w) was not significantly different to that of a square inlet. With increasing size of the inlet configurations, the observed vena contracta became smaller in each configuration (0.10 w and 0.15 w), with the rounded and 45° setup utilizing a greater flow area (the entire cross-sectional area of the culvert) than the other configurations. The round configuration utilized the greatest flow area in all sizes. The round 0.15 w size performed better than all larger (0.20 w and 0.25 w) chamfer configurations. Figure 2 is a visual representation of the velocity distribution. The worst possible case is when the contrast between low flow velocities and high flow velocities was greatest; in other words, the constriction of flow was the highest, as $Q_{in} = Q_{out}$, and therefore, $\int_{y_{in}} v_{in}\, \mathrm{d}y_{in} = \int_{y_{out}} v_{out}\, \mathrm{d}y_{out}$. Correspondingly, a more or less uniform transverse distribution of the flow velocity is an index of the optimality in the inlet design.

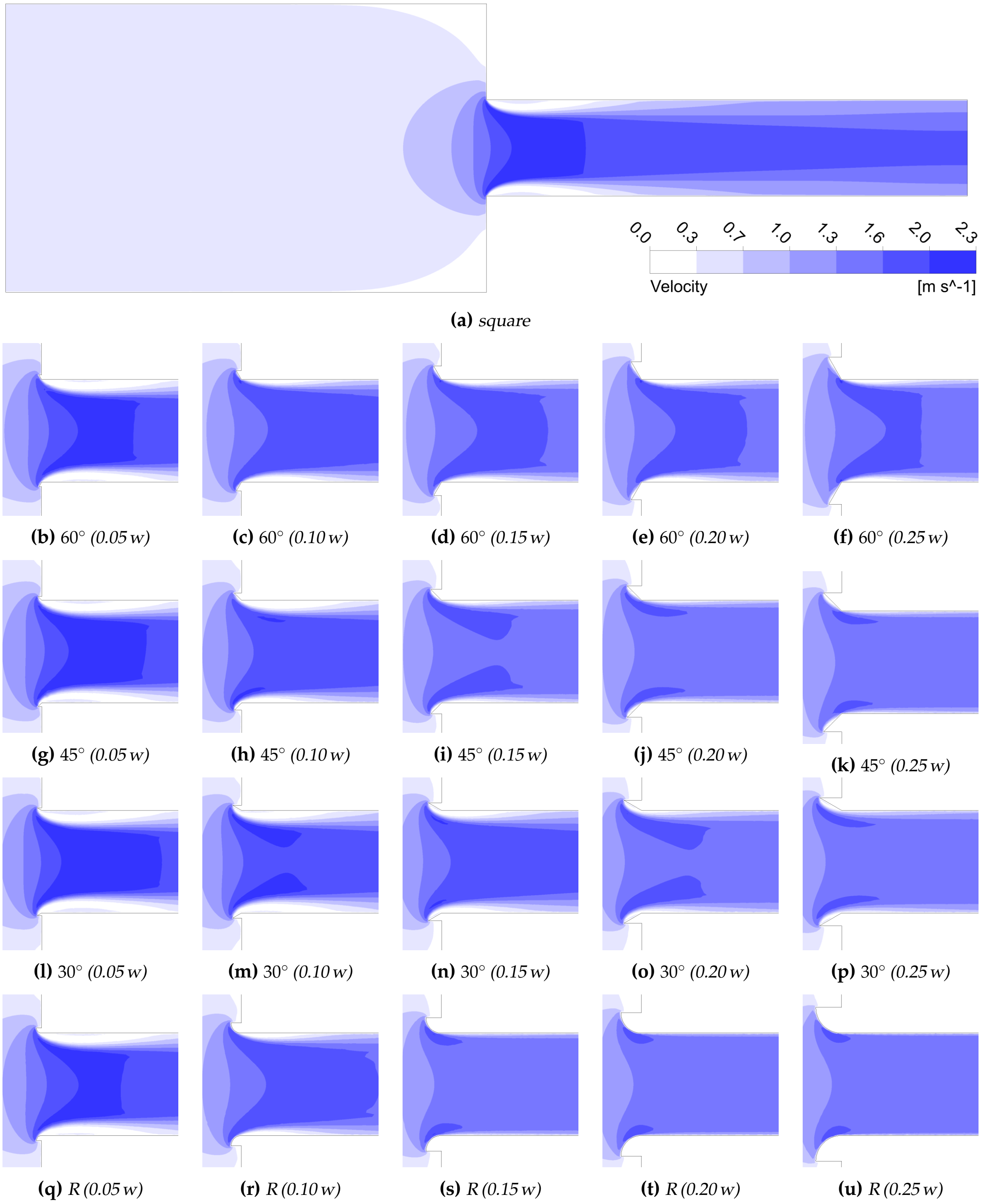

Figure 2. Comparison between velocity contours (**b**–**p**) for chamfered inlets with different angles and (**q**–**u**) for rounded inlets.

Results where the difference between very high and very low velocities was least indicated greater discharge potential as the constriction was minimal. Small changes to inlet shapes showed no real improvement (Figure 2b,g,l,q) and performed similarly to the standard square inlet corners. The 60° setups (Figure 2b–f) had the highest peak velocities in the centre jet of the four different variations. The rounded corners (Figure 2s–u) performed best, having lower peak velocities, followed by the larger 45° setups (Figure 2j,k). It should be noted that the rounded inlets improved the flows noticeably in Figure 2s with similar results in the larger configurations (Figure 2t,u).

Turbulent kinetic energy (TKE) indicates losses in a fluid flow due to eddies caused by shear, friction or buoyancy forces. The darker and larger the areas of TKE in Figure 3, the higher the inlet losses. Again, as seen in Figures 2 and A2, the smallest inlet configuration changes (Figure 3b,g,l,q) showed no significant difference from the standard (*square*) inlet configuration (Figure 3a). All 30° and 60° chamfer setups showed areas of energy losses behind the actual inlet, indicating eddies being formed within the culvert caused by the inlet (Figure 3c–f,m–p). The larger 45° configurations had smaller energy losses than the other chamfered inlets (Figure 3j,k), but the medium and large-sized round inlets performed better, as there were no losses due to TKE (Figure 3s–u).

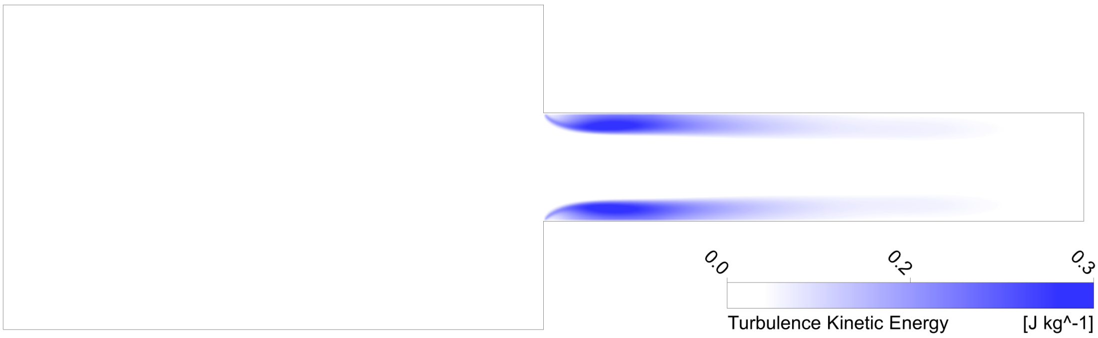

(a) *square*

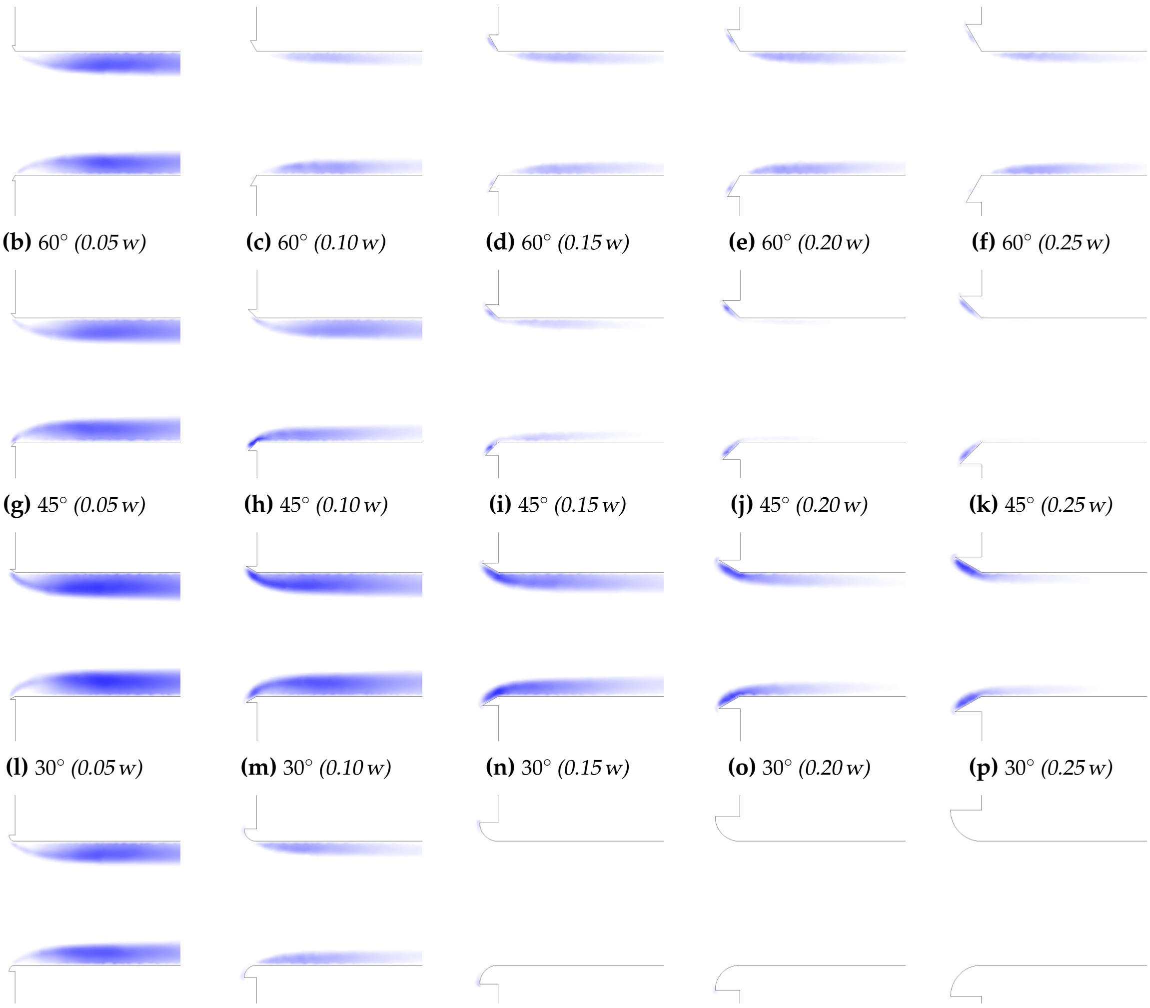

(b) 60° *(0.05 w)* **(c)** 60° *(0.10 w)* **(d)** 60° *(0.15 w)* **(e)** 60° *(0.20 w)* **(f)** 60° *(0.25 w)*

(g) 45° *(0.05 w)* **(h)** 45° *(0.10 w)* **(i)** 45° *(0.15 w)* **(j)** 45° *(0.20 w)* **(k)** 45° *(0.25 w)*

(l) 30° *(0.05 w)* **(m)** 30° *(0.10 w)* **(n)** 30° *(0.15 w)* **(o)** 30° *(0.20 w)* **(p)** 30° *(0.25 w)*

(q) *R (0.05 w)* **(r)** *R (0.10 w)* **(s)** *R (0.15 w)* **(t)** *R (0.20 w)* **(u)** *R (0.25 w)*

Figure 3. Comparison for TKE (**b**–**p**) for chamfered inlets with different angles and (**q**–**u**) for rounded inlets (all sizes in mm).

The sum of TKE from every simulation is plotted in Figure 4. While the round inlets caused the least turbulence, the 30° chamfered inlets showed the highest turbulence. The 45° chamfers followed a clear downward trend, as did the round and 30° ones, but the 60° inlet modifications showed little difference in total TKE. The unmodified square corner had a much higher level of total TKE with 2173 m s^{-2}.

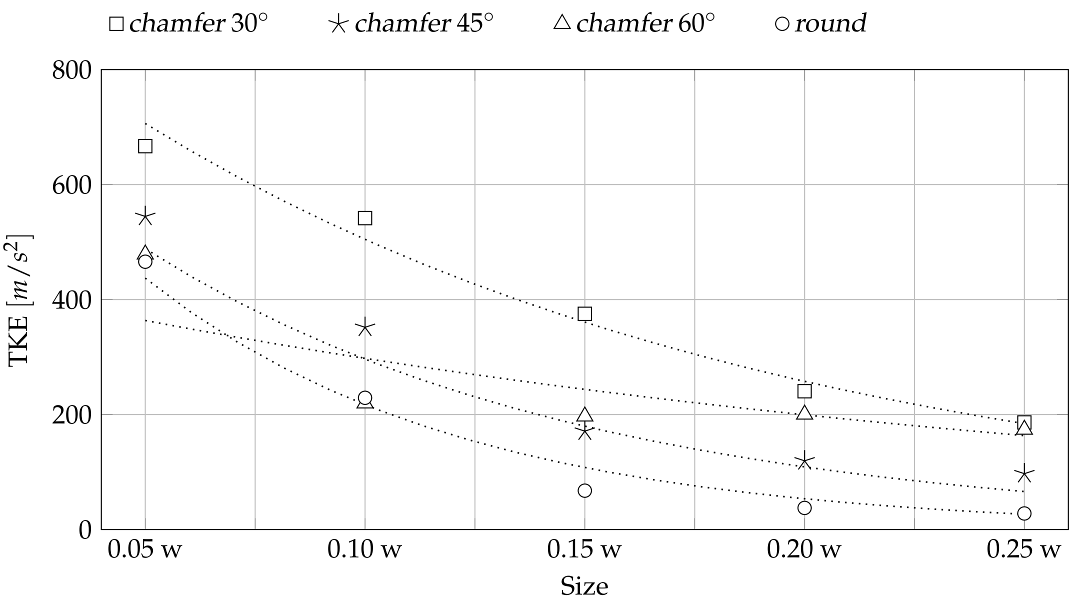

Figure 4. Total TKE for different inlet sizes and cases.

The visualization of streamlines, velocity fields and TKE revealed that flow improvements depended on both shape and size, in order to be effective.

Since the vena contracta reflected the inlet configuration, the velocity distribution at the greatest constriction was investigated. For a better visualization of velocities in 2D graphs, the vectors were separated in their x- and y-directions. Due to a fixed velocity at the inlet, the area under each curve was the same. An even $\vec{x}$-velocity distribution with small peaks is preferable for good performance, as there is little influence from the inlet corners (Figure 5). Ideally, all $\vec{y}$-velocities should be close to zero for the same reason (Figure 6).

Figure 5 shows a comparison of the velocity distributions in the $\vec{x}$-direction for all tested scenarios. Small changes to the inlet shape had little effect on flow performance, giving results similar to the square configuration. Only the larger (0.15 w to 0.25 w) showed considerable improvement.

Velocities in the $\vec{y}$-direction (Figure 6) supported the results shown in Figure 5. All smaller inlet configurations with sizes from 0.05 w to 0.1 w showed opposing peaks in velocity perpendicular to the main flow direction. Results from the 0.15 w to 0.25 w setups were similar in the round and 45° scenarios, but there were greater deviations in the 30° and 60° versions, indicating poorer performance. Figure 6c showed small velocity peaks close to the culvert wall in the 0.10 w to 0.25 w setups. This indicated that eddies and recirculation were present, as the vectors pointed in the direction of the culvert walls. The velocity curves for the 0.15 w to 0.25 w round inlet configurations in Figure 6d, on the other hand, showed the most favourable behaviour. Velocities perpendicular to the main flow direction remained low throughout the culvert width and did not change their direction.

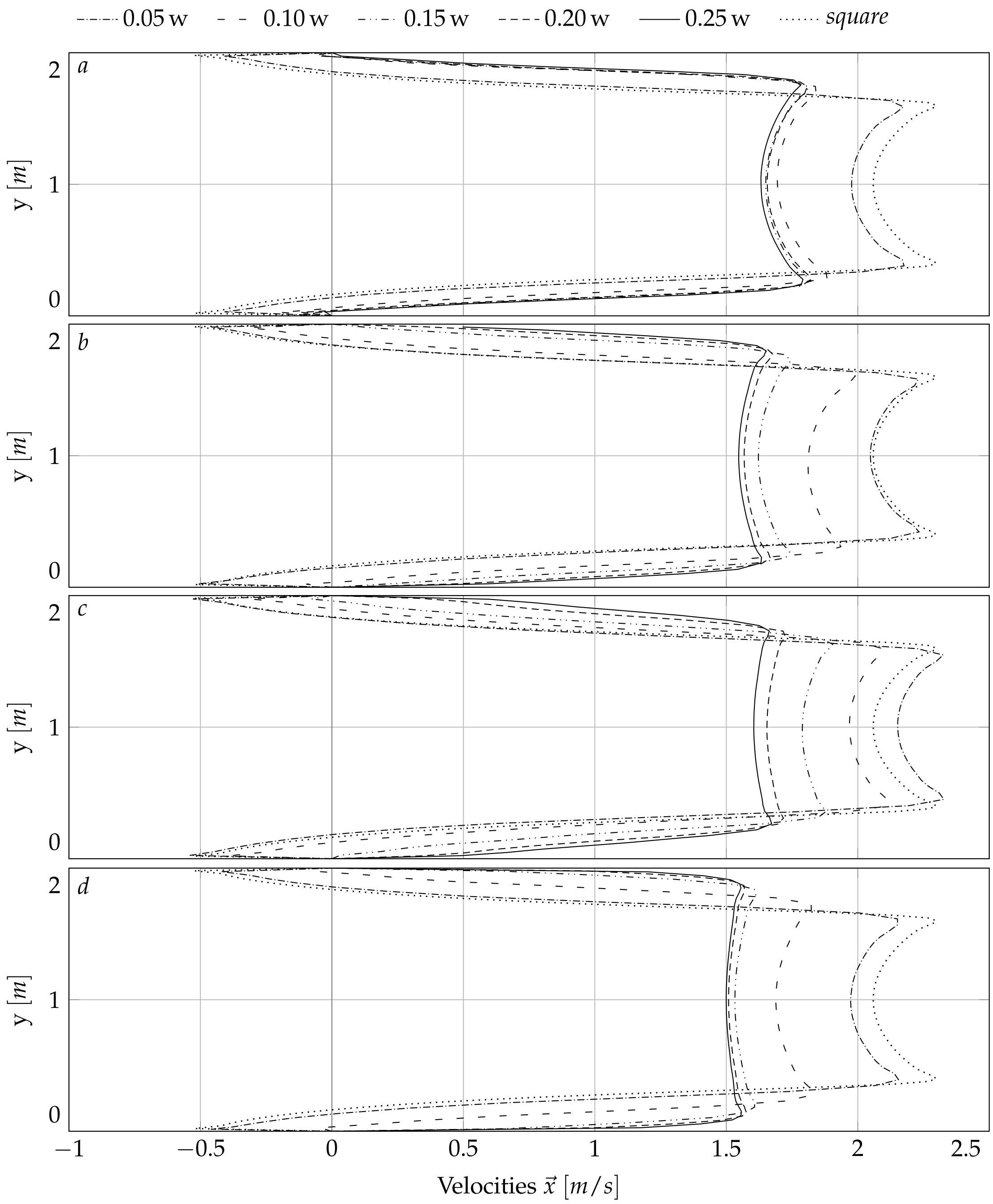

Figure 5. $\vec{x}$-velocity distribution through the culvert 0.7 m after the inlet. (**a**) The 60° chamfer, (**b**) 45° chamfer, (**c**) 30° chamfer and (**d**) rounded.

The largest setups improved the flow the most in all four configurations, although relatively similar results were achieved with the medium-sized setups. The different configurations from the medium and largest setups were compared directly (Figure 7). An expanded x-axis scale elucidates performance differences between the setups.

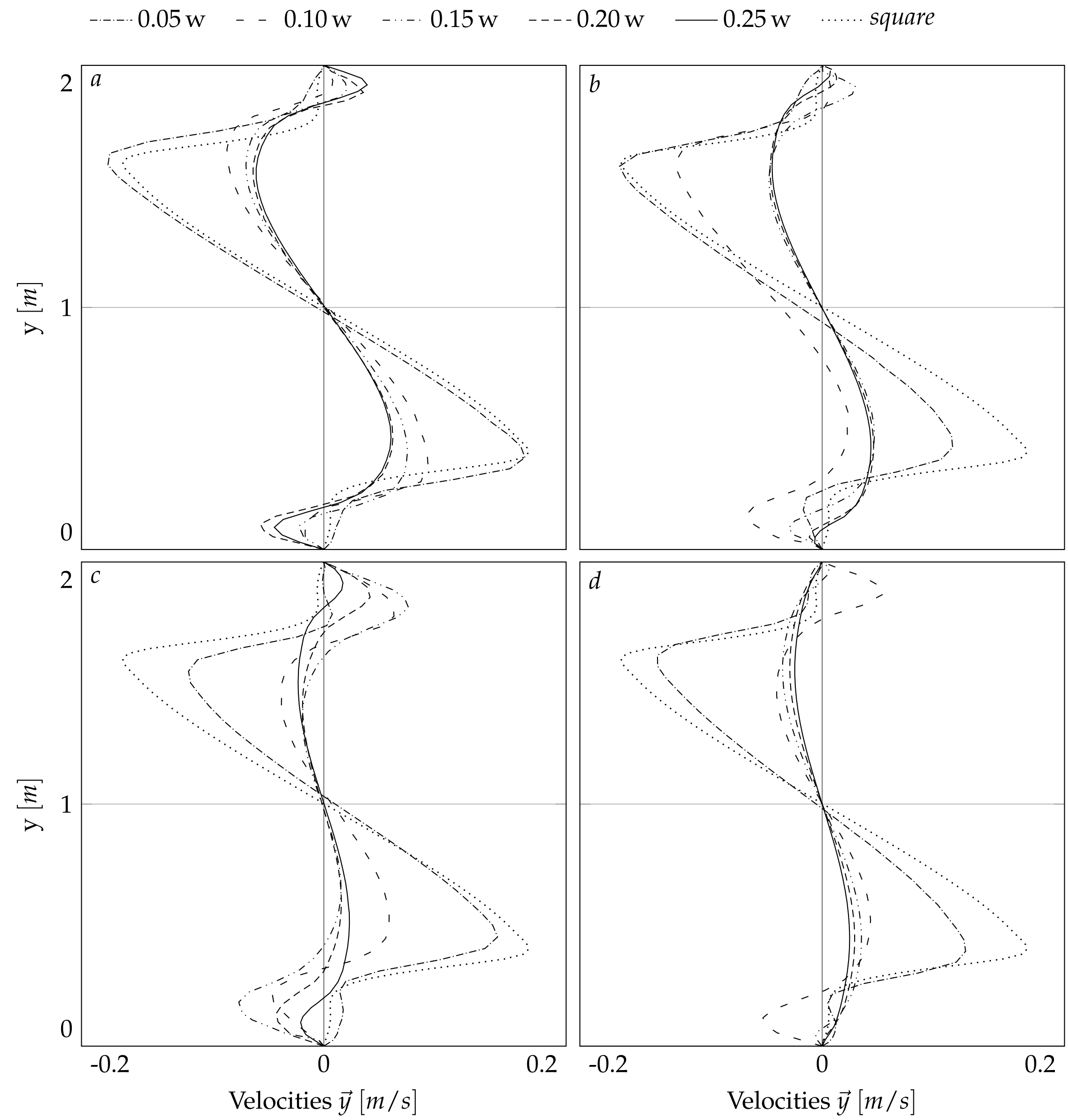

Figure 6. $\vec{y}$-velocity distribution through the culvert 0.7 m after the inlet. (**a**) 60°-chamfer, (**b**) 45°-chamfer, (**c**) 30°-chamfer and (**d**) rounded.

3.2. Experimental Flume Results

Experiments in the flume were carried out to validate the results of the CFD modelling. A small-scale culvert model was tested with two different inlet configurations, the square edge with a straight headwall, and the 0.20 w round one. Figure 8 illustrates the different headwater levels between square and round inlets. The results are displayed as dimensionless values with a Froude similarity conversion according to [41]. The relative energy head is written as h/D and the non-dimensional flow rate Q^* is defined as $Q^* = Q\left(g \times D^5\right)^{-0.5}$.

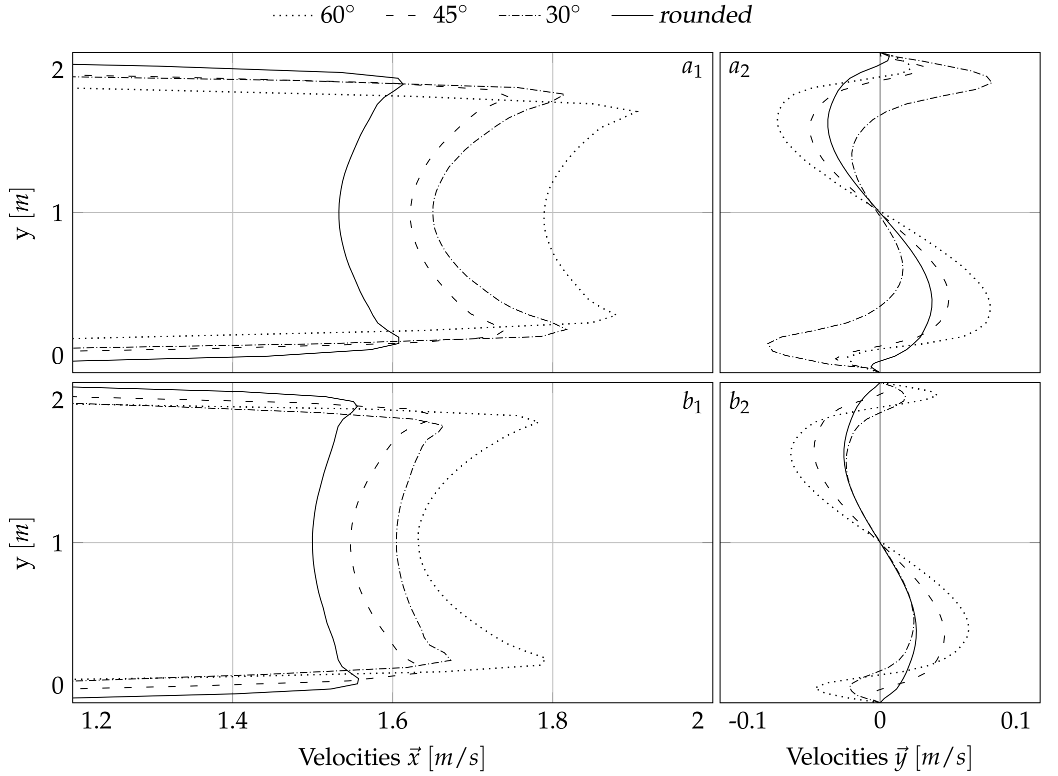

Figure 7. $\vec{x}$ and $\vec{y}$-velocity distributions through the culvert 0.7 m after the inlet. (**a**) for 0.15 w setups and (**b**) for 0.25 w setups.

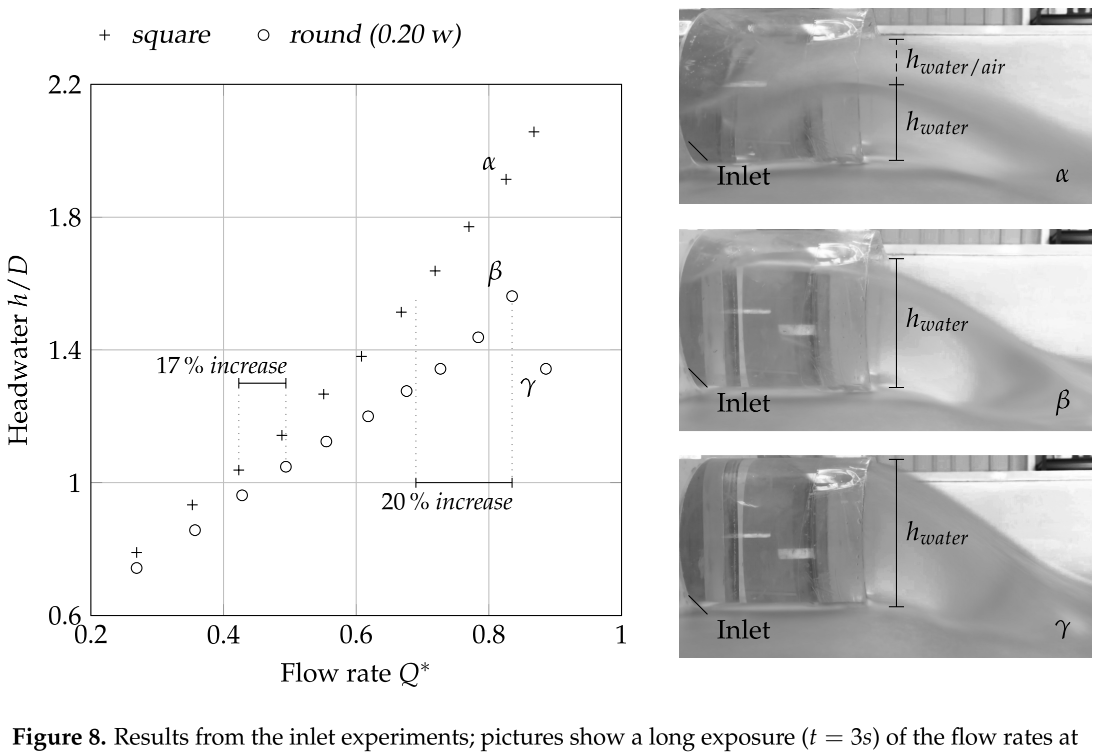

Figure 8. Results from the inlet experiments; pictures show a long exposure ($t = 3s$) of the flow rates at the points α–γ in side view. The water level exiting the culvert is annotated; ($\boldsymbol{\alpha}$) square inlet corners at 9.3 L s^{-1}; air entrainment causes blurred limits of the outflow; ($\boldsymbol{\beta}$) round inlet corners at 9.3 L s^{-1}; air is entering the culvert through vortices forming at the inlet; (γ) round inlet corners at 10 L s^{-1}; no air is entering the culvert any more; the short pipe section is completely filled with water.

The round inlet modifications improved the discharge capacity compared to square inlet corners with a straight headwall. For submerged flow conditions, the flow rates increased up to 20%.

At 9.3 $\mathrm{L\,s^{-1}}$, the square inlet corners caused highly turbulent flow conditions and air entrainment, reducing the discharge, while the same flow rate with rounded inlet corners showed less turbulence and higher water levels within the pipe, i.e., less air entrainment. At a higher flow rate, 10 $\mathrm{L\,s^{-1}}$, the air remaining in the pipe was displaced from within the pipe (Figure 8). At the same time, the headwater level dropped 35 % in comparison to the square inlet. Calculating the discharge coefficient C_d for the two different setups, from 6 $\mathrm{L\,s^{-1}}$ to 9.5 $\mathrm{L\,s^{-1}}$, showed arithmetic mean values from $C_d = 0.59$ for the square inlet and $C_d = 0.69$ for the round inlet.

4. Discussion

Four different retrofit options for stormwater culverts were analysed with the aim of increasing flow rates and informing future designs. The numerical simulations revealed that the larger inlet retrofit options, with a 45° chamfer or rounded inlets, improved the flows the most. The length/radius of those modifications should be at least 15 % of the total culvert width on each side. From a hydraulic perspective, the rounded inlet was superior to chamfered inlets and gave the best overall performance. The round, medium-sized (0.15 w) option improved the flow more than the large (0.25 w) chamfer option.

The 45° chamfer retrofit might be a viable alternative to round inlet configurations because it improved the flow more than the two other tested chamfer angles, and its straight geometry had the advantage of requiring a less complex concrete formwork. Large (0.25 w) 45° chamfer retrofits achieved nearly the same performance as the 0.15 w round corners (Figure 7). The largest (0.25 w) 30° and 60° chamfer setups caused higher velocity jets and more constriction to flow than the medium-sized round inlets (0.15 w); therefore, these configurations would be unsuitable. The smallest size of the inlet configurations (0.05 w) improved the flow slightly, but not to any practical extent (Figures 5 and 6).

Research by Jones et al. [19] supported these findings, although their experiments were limited to box culverts and relatively small inlet modifications. The ≈100 mm (4 in) and ≈200 mm (8 in) configurations were tested in 1.83 m (6 ft) openings, resulting in inlet modifications being only 5.5 % and 11 % of the total culvert width. Our study showed that there was a further performance increase using sizes of at least 15 % of the culvert size.

A greater improvement might have been achieved by integrating the inlet modifications into the headwall, avoiding a setup that projects out into the flow. Instead, all configurations were added to the headwall in order to model retrofit solutions. This setup created projecting inlets, especially at small angles (30°), and these inlets are among the least efficient configurations [14,20]. This is caused by the greater turning angle the water has to follow before entering the inlet. With thin projecting inlets, there is the potential for greater direction changes than 90°, which is the maximum for inlets with rectangular corners. The larger the inlet modifications, the greater the length for the change of direction and the smaller the influence of this effect.

Flume experiments with a small-scale culvert model compared two different inlet configurations. The experimental results, which arose from comparing a rounded inlet to that of a square corner with a straight headwall, agreed with the simulations.

However, the experimental setup and the large scaling factor can affect the results, and although we converted the data to non-dimensional values, the real-world applications might not achieve as good results as the flume experiments. There are two reasons for this. The first one is that the smooth Perspex surface and the short pipe in the experiments caused very little pipe friction losses, which differed from actual culverts. Higher pipe losses caused by rougher materials can potentially force culverts from inlet to outlet control. This could limit the potential of the proposed approach as the pipe friction becomes the new limiting factor of the discharge potential. The second reason is that scaling itself affects the hydraulic conditions and therefore the results [41–43]. The Froude similarity conversion that we used is supposed to incorporate these scaling effects.

The drop in headwater levels between the points β and γ (Figure 8), due to the transition from a free surface flow in the pipe to a full flowing pipe, needs further investigation. An earlier transition could increase the discharge capacity even further.

5. Conclusions

The experiments showed that altered inlet corners can improve the flow rates in pipes substantially. In this regard, large rounded inlets, or 45° chamfers, performed best during simulations. The inlet design is one of the restricting factors in culvert flows, so minimizing its impact facilitates higher discharge capacities. All suggested modifications can be installed as retrofit solutions to increase flow rates in flood-prone structures. While most of the solutions will increase the discharge capacity, round inlet corners were found to be the most effective. The radius of the rounded corners should be at least 15 % of the culvert width. Large chamfers with 45° angles can also increase flow rates significantly. Future research should investigate other chamfer angles and their impact on flow rates, as well as determining exact loss coefficients for the proposed inlet configurations. While the suggested inlet shapes can be applied continuously to round culvert shapes, corners found in rectangular culverts need a transition between vertical and horizontal parts to minimize eddies. The approach presented here offers a simple solution to the need for increasing flow rates in those existing structures that are not capable of discharging sufficient amounts of water. Research into hydraulic inlet design has been neglected, but the above approach advances our understanding by maximizing the potential discharge of existing structures. This is essential research as we adapt to the consequences of climate change.

Author Contributions: Conceptualization, formal analysis, investigation, methodology, software, validation, writing, original draft preparation, R.J.; writing, review and editing, R.J., K.T., C.J., M.P. and N.T.; supervision, K.T., C.J., M.P. and N.T.

Funding: A scholarship and operational funds were provided by the Sunshine Coast Council, and we very much appreciate their support.

Conflicts of Interest: The authors declare no conflict of interest.

Abbreviations

The following abbreviations are used in this manuscript:

CFD	computational fluid dynamics
MEL	minimum energy loss (culverts)
RANS	Reynolds averaged Navier–Stokes
TKE	turbulent kinetic energy
α	angle
C_d	discharge coefficient
D	diameter
h	height
l	length
Q^*	non-dimensional flow rate
r	radius
v	velocity
w	width (culvert)

Appendix A

Appendix A.1. Methods

Table A1. Applied meshing parameters in ANSYS Fluent: summary of alterations made to the standard setup.

Defaults	
Physics preference	CFD
Solver preference	Fluent
Sizing	
Use advanced size function	On: proximity and curvature
Relevance centre	Fine
Initial size seed	Active assembly
Smoothing	High
Span angle centre	Fine
Max face size	0.05 m
Max size	0.05 m
Inflation	
Scoping method	Geometry selection (- -) 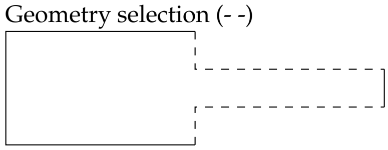
Type	Element size
Element size	0.02 m
Behaviour	Soft

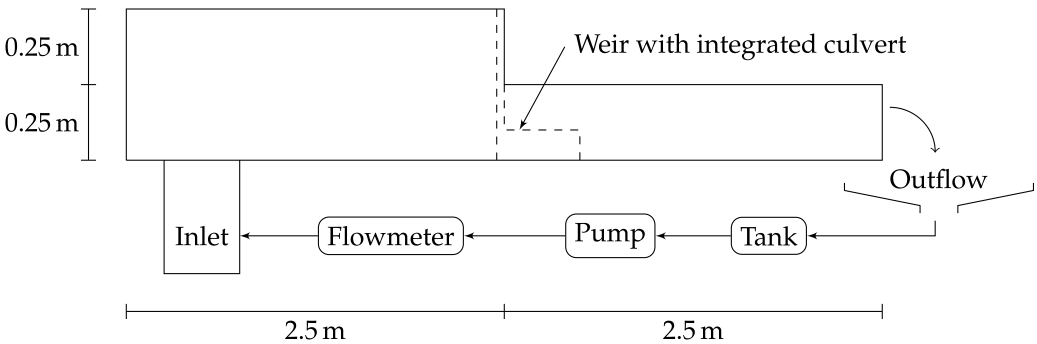

Figure A1. Schematic side view of the experimental flume.

Appendix A.2. Results

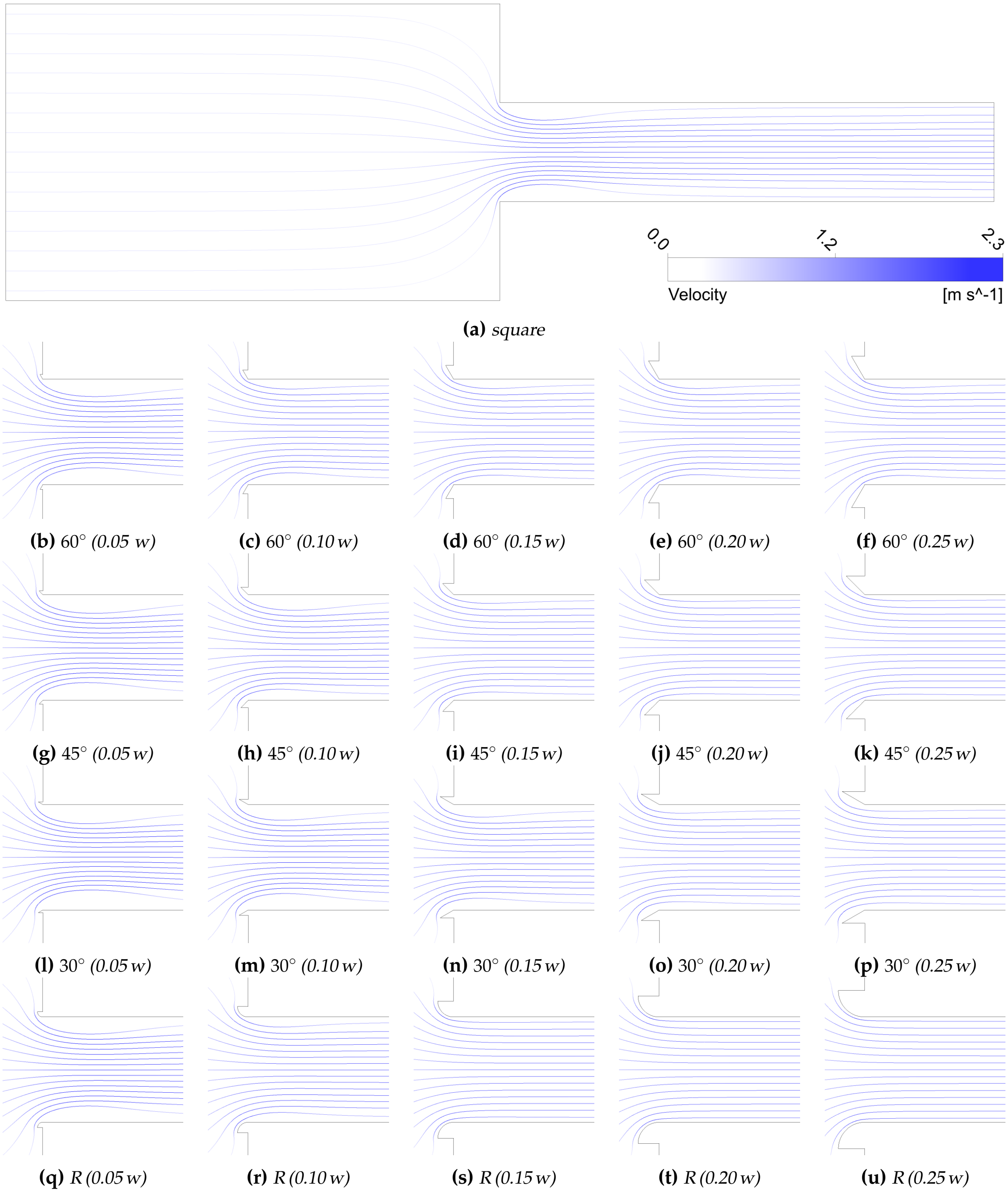

(a) *square*

(b) 60° *(0.05 w)* **(c)** 60° *(0.10 w)* **(d)** 60° *(0.15 w)* **(e)** 60° *(0.20 w)* **(f)** 60° *(0.25 w)*

(g) 45° *(0.05 w)* **(h)** 45° *(0.10 w)* **(i)** 45° *(0.15 w)* **(j)** 45° *(0.20 w)* **(k)** 45° *(0.25 w)*

(l) 30° *(0.05 w)* **(m)** 30° *(0.10 w)* **(n)** 30° *(0.15 w)* **(o)** 30° *(0.20 w)* **(p)** 30° *(0.25 w)*

(q) *R (0.05 w)* **(r)** *R (0.10 w)* **(s)** *R (0.15 w)* **(t)** *R (0.20 w)* **(u)** *R (0.25 w)*

Figure A2. Streamlines with different inlet configurations: (**b**–**p**) for chamfered inlets with different angles, (**q**–**u**) for rounded inlets (all sizes in mm).

References

1. French, J.L. *First Progress Report on Hydraulics of Short Pipes: Hydraulic Characteristics of Commonly Used Pipe Entrances*; NBS Report; U.S. Dept. of Commerce, National Bureau of Standards: Washington, DC, USA, 1955; Volume 4444.
2. French, J.L. *Second Progress Report on Hydraulics of Culverts: Pressure and Resistance Characteristics of a Model Pipe Culvert*; NBS Report; U.S. Dept. of Commerce, National Bureau of Standards: Washington, DC, USA, 1956; Volume 4911.
3. French, J.L. *Third Progress Report on Hydraulics of Culverts: Effect of Approach Channel Characteristics on Model Pipe Culvert Operation*; NBS Report; U.S. Dept. of Commerce, National Bureau of Standards: Washington, DC, USA, 1957; Volume 5306.
4. French, J.L. *Fourth Progress Report on Hydraulics of Culverts: Hydraulics of Improved Inlet Structures for Pipe Culverts*; NBS Report; U.S. Dept. of Commerce, National Bureau of Standards: Washington, DC, USA, 1961; Volume 7178.
5. French, J.L. *Fifth Progress Report on Hydraulics of Culverts Nonenlarged Box Culvert Inlets*; NBS Report; NBS: Washington, DC, USA, 1966; Volume 9327.
6. French, J.L. *Sixth Progress Report on Hydraulics of Culverts: Tapered Box Culvert Inlets*; NBS Report; U.S. Dept. of Commerce, National Bureau of Standards: Gaithersburg, MD, USA, 1966; Volume 9355.
7. French, J.L.; Bossy, H.G. *Seventh Progress Report on Hydraulics of Culverts: Tapered Box Culvert Inlets with Fall Concentration in the Inlet Structure*; National Bureau of Standards: Washington, DC, USA, 1967.
8. Bodhaine, G.L. Measurement of Peak Discharge at Culverts by Indirect Methods. In *Techniques of Water-Resources Investigations of the United States Geological Survey*; U.S. G.P.O: Washington, DC, USA, 1968; Volume 3, Chapter A3.
9. Apelt, C.J. Hydraulics of Minimum Energy Culverts and Bridge Waterways. *Aust. Civ. Eng. Trans. I. E. Aust.* **1983**, *CE25*, 89–95.
10. House, M.R.; Pyles, M.R.; White, D. Velocity distributions in streambed simulation culverts used for fish passage. *J. Am. Water Resour. Assoc.* **2005**, *41*, 209–217. [CrossRef]
11. Paik, J.; Park, S.D. (Eds.) Numerical Simulation of Flood and Debris Flows through Drainage Culvert. *Ital. J. Eng. Geol. Environ. Book* **2011**, *11*, 487–493. [CrossRef]
12. Feurich, R.; Boubée, J.; Olsen, N. Improvement of fish passage in culverts using CFD. *Ecol. Eng.* **2012**, *47*, 1–8. [CrossRef]
13. Ball, J.; Babister, M.; Nathan, R.; Weeks, W.; Weinmann, E. *Australian Rainfall and Runoff: A Guide to Flood Estimation*; Commonwealth of Australia (Geoscience Australia): Symonston, Australia, 2016.
14. Schall, J.D.; Thompson, P.L.; Zerges, S.M.; Kilgore, R.T.; Morris, J.L. *Hydraulic Design of Highway Culverts*, 3rd ed.; Hydraulic Design Series; U.S. Dept. of Transportation, Federal Highway Administration: Washington, DC, USA, 2012; Volume 5.
15. Deutsches Institut für Normung e.V. *Hydraulic structures—Part 1: Crossing Works, Culvert Works and Drain Works*; Deutsches Institut für Normung (DIN): Berlin, Germany, 1998.
16. Straub, L.G. *Importance of Inlet Design on Culvert Capacity*; University of Minnesota: Minneapolis, MN, USA, 1953.
17. Day, R.A. Preliminary observations of turbulent flow at culvert inlets. *J. Hydraul. Eng.* **1997**, *123*, 116–124. [CrossRef]
18. Chanson, H. Introducing originality and innovation in engineering teaching: The hydraulic design of culverts. *Eur. J. Eng. Educ.* **2000**, *25*, 377–391. [CrossRef]
19. Jones, J.S.; Kerenyi, K.; Stein, S. *Effects of Inlet Geometry on Hydraulic Performance of Box Culverts: Laboratory Report*; U.S. Dept. of Transportation, Federal Highway Administration, Turner-Fairbank Highway Research Center: McLean, VA, USA, 2004.
20. Hunt, M.; Clark, S.; Tkach, R. Velocity distributions near the inlet of corrugated steel pipe culverts. *Can. J. Civ. Eng.* **2012**, *39*, 1243–1251. [CrossRef]
21. Kolerski, T.; Wielgat, P. Velocity field characteristics at the inlet to a pipe culvert. *Arch. Hydroeng. Environ. Mech.* **2014**, *61*, 127–140. [CrossRef]
22. Guven, A.; Hassan, M.; Sabir, S. Experimental investigation on discharge coefficient for a combined broad crested weir-box culvert structure. *J. Hydrol.* **2013**, *500*, 97–103. [CrossRef]

23. Olsen, A.H.; Tullis, B.P. Laboratory Study of Fish Passage and Discharge Capacity in Slip-Lined, Baffled Culverts. *J. Hydraul. Eng.* **2013**, *139*, 424–432. [CrossRef]
24. Blanc, J.; Wallerstein, N.P.; Wright, G.B.; Arthur, S. Analysis of the performance of debris screens at culverts. *Proc. Inst. Civ. Eng. Water Manag.* **2014**, *167*, 219–229. [CrossRef]
25. McKay, G.R. *Design of Minimum Energy Culverts*; University of Queensland, Department of Civil Engineering: St Lucia, Australia, 1971.
26. Arnbjerg-Nielsen, K.; Willems, P.; Olsson, J.; Beecham, S.; Pathirana, A.; Bülow Gregersen, I.; Madsen, H.; Nguyen, V.T.V. Impacts of climate change on rainfall extremes and urban drainage systems: A review. *Water Sci. Technol. J. Int. Assoc. Water Pollut. Res.* **2013**, *68*, 16–28. [CrossRef] [PubMed]
27. Peters, G.P.; Andrew, R.M.; Boden, T.; Canadell, J.G.; Ciais, P.; Le Quéré, C.; Marland, G.; Raupach, M.R.; Wilson, C. The challenge to keep global warming below 2 degree C. *Nat. Clim. Chang.* **2013**, *3*, 4–6. [CrossRef]
28. Wasko, C.; Sharma, A. Global assessment of flood and storm extremes with increased temperatures. *Sci. Rep.* **2017**, *7*, 7945. [CrossRef] [PubMed]
29. Hettiarachchi, S.; Wasko, C.; Sharma, A. Increase in flood risk resulting from climate change in a developed urban watershed—The role of storm temporal patterns. *Hydrol. Earth Syst. Sci.* **2018**, *22*, 2041–2056. [CrossRef]
30. Verstraten, L.; Wasko, C.; Ashford, G.; Sharma, A. Sensitivity of Australian roof drainage structures to design rainfall variability and climatic change. *Build. Environ.* **2019**, *161*, 106230. [CrossRef]
31. Kilgore, R.T.; Bergendahl, B.S.; Hotchkiss, R.H. *Culvert Design for Aquatic Organism Passage*, 1st ed.; Hydraulic Engineering Circular; U.S. Federal Highway Administration, Central Federal Lands Highway Division: Lakewood, CO, USA, 2010; Volume 26.
32. Yazdanfar, Z.; Sharma, A. Urban drainage system planning and design–challenges with climate change and urbanization: A review. *Water Sci. Technol. J. Int. Assoc. Water Pollut. Res.* **2015**, *72*, 165–179. [CrossRef]
33. Zahmatkesh, Z.; Karamouz, M.; Goharian, E.; Burian, S.J. Analysis of the Effects of Climate Change on Urban Storm Water Runoff Using Statistically Downscaled Precipitation Data and a Change Factor Approach. *J. Hydrol. Eng.* **2015**, *20*, 05014022. [CrossRef]
34. Kang, N.; Kim, S.; Kim, Y.; Noh, H.; Hong, S.; Kim, H. Urban Drainage System Improvement for Climate Change Adaptation. *Water* **2016**, *8*, 268. [CrossRef]
35. ANSYS Fluent. *Theory Guide*; Ansys Inc.: Canonsburg, PA, USA, 2015.
36. Boussinesq, J. *Théorie Analytique de la Chaleur*; Gauthier-Villars: Paris, France, 1921.
37. Jones, W.P.; Launder, B.E. The prediction of laminarization with a two-equation model of turbulence. *Int. J. Heat Mass Transf.* **1972**, *15*, 301–314. [CrossRef]
38. Larsson, I.A.S.; Lindmark, E.M.; Lundström, T.S.; Nathan, G.J. Secondary Flow in Semi-Circular Ducts. *J. Fluids Eng.* **2011**, *133*, 101206. [CrossRef]
39. Launder, B.E.; Spalding, D.B. The numerical computation of turbulent flows. *Comput. Methods Appl. Mech. Eng.* **1974**, *3*, 269–289. [CrossRef]
40. Turner, B.N.; Gold, S.A. A review of melt extrusion additive manufacturing processes: II. Materials, dimensional accuracy, and surface roughness. *Rapid Prototyp. J.* **2015**, *21*, 250–261. [CrossRef]
41. Hager, W.H.; Del Giudice, G. Generalized culvert design diagram. *J. Irrig. Drain. Eng.* **1998**, *124*, 271–274. [CrossRef]
42. Novák, P.; Čábelka, J. *Models in Hydraulic Engineering: Physical Principles and Design Applications*; Monographs and Surveys in Water Resources Engineering; Novák, P., Čábelka, J., Eds.; Pitman: Boston, MA, USA; London, UK, 1981; Volume 4.
43. Heller, V. Scale effects in physical hydraulic engineering models. *J. Hydraul. Res.* **2011**, *49*, 293–306. [CrossRef]